Cardiovasc Eng (2006) 6:95–104
DOI 10.1007/s10558-006-9013-5

ORIGINAL PAPER

A Combined FEM/Genetic Algorithm for Vascular Soft tissue Elasticity Estimation

Ahmad S. Khalil · Brett E. Bouma · Mohammad R. Kaazempur Mofrad

Published online: 12 September 2006

Abstract Tissue elasticity reconstruction is a parameter estimation effort combining imaging, elastography, and computational modeling to build maps of soft tissue mechanical properties. One application is in the characterization of atherosclerotic plaques in diseased arteries, wherein the distribution of elastic properties is required for stress analysis and plaque stability assessment. In this paper, a computational scheme is proposed for elasticity reconstruction in soft tissues, combining finite element modeling (FEM) for mechanical analysis of soft tissues and a genetic algorithm (GA) for parameter estimation. With a model reduction of the discrete elasticity values into lumped material regions, namely the plaque constituents, a robust, adaptive strategy can be used to solve inverse elasticity problems involving complex and inhomogeneous solution spaces. An advantage of utilizing a GA is its insistence on global convergence. The algorithm is easily implemented and adaptable to more complex material models and geometries. It is meant to provide either accurate initial guesses of low-resolution elasticity values in a multi-resolution scheme or as a replacement for failing traditional elasticity estimation efforts.

A. S. Khalil · M. R. Kaazempur Mofrad (✉)
Department of Bioengineering, University of California, 483 Evans Hall #1762, Berkeley, CA 94720, USA
e-mail: mofrad@berkeley.edu

A. S. Khalil
Department of Mechanical Engineering, Massachusetts Institute of Technology, Cambridge, MA 02139, USA

B. E. Bouma
Wellman Center for Photomedicine, Massachusetts General Hospital, Harvard Medical School, Boston, MA 02114, USA

Keywords Soft tissue · Elasticity reconstruction · Atherosclerosis · Optical coherence tomography · Genetic algorithm · FEM

Introduction

Deducing the mechanical properties of specimens under realistic boundary conditions is challenging, not merely because it does not allow for use of the classical methods but because it generally involves materials with inhomogeneous field data. Knowledge of the boundary conditions, therefore, is not sufficient. For these types of specimens, and biomaterials often fall into this category, measurements of field information (displacement, stress, strain) are necessary. Researchers have modeled a wide variety of biological tissues, including articular cartilage and the meniscus (Mow et al. 1980), skin and subcutis (Oomens et al. 1987), and the myocardium (Costa et al. 2001), in attempts to describe their mechanical behavior for medical and therapeutic purposes. Nonetheless, knowledge of the material properties of soft tissues remains limited (Ophir et al. 1996) partly a result of specimen and experimental variability—the elastic moduli of normal soft tissue span four orders of magnitude (Duck 1990; Sarvazyan 1993) Yet, a better understanding of this variability in the form of quantifiable field maps of material properties would be of valuable consequence.

This endeavor is certainly appreciated by those attempting to diagnose cardiovascular disease based on the mechanical behavior of diseased arterial tissue. Most commonly a result of atherosclerosis, an inflammatory process leading to arterial stenosis, cardiovascular

disease is associated with numerous life-threatening events, such as myocardial infarction and stroke, *especially* after spontaneous rupture of *structurally vulnerable* plaques. Not surprisingly, it continues to be the principal cause of morbidity and mortality in industrialized countries (American Heart Association 2003).

The hunt for a reliable means of patient-specific plaque detection has recently migrated toward biomechanical analysis of plaque matter and rupture. Unfortunately, there is still a dearth of data on the mechanical behavior and properties of soft arterial tissue (Cheng et al. 1993; Humphre 1995; Loree et al. 1994). The ability to quantify vulnerable plaque mechanical properties, however, would provide (i) maps and locations of high stress concentration, which have been shown to correspond with regions where plaque rupture tends to occur (Richardson et al. 1989) and (ii) distributions of the mechanical stresses being applied to vascular cells, which could elucidate the biochemical responses and mechanotransduction pathways associated with atherogenesis.

Tissue elasticity reconstruction combines imaging, elastography, and modeling to generate specimen-specific elasticity distributions. Blood vessels, for example, are imaged via invasive and/or non-invasive modalities, where the invasive sort, such as intravascular ultrasound (IVUS) (de Korte et al. 2000) and optical coherence tomography (OCT) (Chan et al. 2004; Chau et al. 2004; Yabushita et al. 2002) are well suited for coronary arteries *in vivo*, while the noninvasive, such as magnetic resonance imaging (MRI) (Yuan et al. 1994) and peripheral vascular ultrasound (de Bray et al. 1997) are intended for larger arteries, such as carotids. In addition to providing geometry and plaque morphology, imaging is used as a scaffold for elastography experiments, where subsequent images of a tissue being displaced are translated to displacement and strain maps. Since the inception of ultrasound-based tissue elastography (Ophir et al. 1991), this technique has been widely researched and extended to other imaging modalities, including to intravascular ultrasound (IVUS), which remains the only clinically-demonstrated method for strain characterization of coronary lesions (de Korte et al. 2000). However, elastograms are only an incomplete view of a specimen's mechanical properties, as no technique exists for measuring internal stress. Since our ultimate goal is the diagnosis of stress concentrations, especially at tissue boundaries where elastograms can be unhelpful (Ponnekanti et al. 1995), we must solve the inverse elasticity problem.

In this work, we review the inverse elasticity problem and propose a non-gradient-based scheme for solving it. Traditionally, researchers have approximated gradient search directions in order to minimize a residual between measured and computed mechanical responses (Doyley et al. 2000; Kallel and Bertrand 1996). In some cases, however, an approximation for the gradient may be faulty and can lead to inefficient and ineffective convergence patterns. This is especially true for problems that exhibit complex and inhomogeneous solution spaces or where *a priori* initial guesses of the elasticity are unreliable. Because the goal of gradient-based techniques is to determine a search direction, they are clearly the most efficient when successful; however, the solution space may not always allow for the approximation of smooth and accurate gradients. For these cases, we show that a genetic algorithm can very easily be implemented to solve the elasticity estimation problem and then apply it to a variety of vascular phantom models.

Methods

Inverse elasticity problem

Most biological soft tissues, especially arterial walls, are accurately represented with hyperelastic constitutive models, where strain energy functions are formulated to capture the nonlinear nature of the stress–strain curve at high strains. Within the realm of elasticity estimation, however, researchers tend to rely on the simpler, more direct linear elastic, isotropic model so long as the limits of the results of such estimation are understood. The incompressible linear elastic stress–strain constitutive relations under isotropic and plane-strain assumptions are known to sufficiently model the behavior of the tissue undergoing *small*, *quasi-static deformations* (Ophir et al. 1996). In this proof of principle work, we begin with linear elasticity to make computation more feasible, and will leave more complex constitutive models for future works.

A body being deformed by an external load or displacement is described by its constitutive relationship and by stress equilibrium. It is assumed that each point on the boundary of the solid is specified either by a stress or displacement and that $v(x,y,z)$ denotes the displacement field as a function of spatial coordinates (x,y,z). Assuming incompressibility, we write for a linear elastic solid,

$$\sigma_{ij} = -p\delta_{ij} + 2\mu\varepsilon_{ij}, \tag{1}$$

where σ_{ij} is a component of the stress tensor, μ is the material shear modulus, p is the pressure or hydrostatic stress, and δ_{ij} is the Kronecker delta. Stress equilibrium is satisfied by balancing linear momentum over each part of the material,

$$\frac{\partial \sigma_{ij}}{\partial x_j} + f_j = 0, \tag{2}$$

where f_j, the body force per unit volume, is typically neglected. Combining Eqs. (1) and (2) under the plane strain approximation yields the ''plane strain inversion equation'' for the single unknown shear modulus, μ as follows (Skovoroda et al. 1995)

$$\frac{\partial^2(\varepsilon_{xy}\mu)}{\partial y^2} - \frac{\partial^2(\varepsilon_{xy}\mu)}{\partial x^2} + 2\frac{\partial^2(\varepsilon_{xx}\mu)}{\partial x \partial y} = 0. \tag{3}$$

While this set of partial differential equations is most efficiently solved by direct inversion for the shear modulus, in practice, this strategy is avoided. Solutions are difficult to stabilize and Eq. (3) requires an explicit form for the strain field, which means differentiating the presumably noisy measured displacement field. Additionally, second order partial derivatives of μ appearing in Eq. (3) place continuity restrictions on the unknown modulus field.

Instead, the set of partial differential equations is iteratively inverted by fashioning it into a nonlinear least squares (NLS) problem, where the goal is to minimize a residual between computed and measured mechanical responses (i.e., displacement fields).

The resulting system, known as the Inverse Problem (IP) in elastography, is written as

$$\begin{aligned} &\text{Given} \quad v_c : R^p \rightarrow R^q, q \geq p, \quad \text{solve} \\ &\min_{E \in R^p} \left\{ \Phi(E) = \frac{1}{2} \| v_c(E) - v_a \|^2 \right\}, \end{aligned} \tag{4}$$

where E is the elastic modulus distribution, a one-dimensional vector ($p = 1$) assuming an isotropic distribution, $v_c(E)$ is the vector of computed displacements based on a given E, and v_a is the vector of measured displacements. Although here the IP is written in terms of an unknown distribution E, it can equivalently be written to solve for the shear modulus.

Parameter reduction

Consider a model with m unknown parameters, E_m, yielding a set of output values $g = (g_1,...,g_n)$ that are to be compared with a set of experimentally-determined values $u = (u_1,...,u_n)$, where $m \leq n$. The objective is to accurately estimate the model parameters, based on knowledge of g and u. For the elasticity problem, the unknown parameters manifest themselves in the elastic modulus distribution and the output variables (g and u) the computed and measured displacement fields, respectively. As m approaches n, inverse problems typically become ill-conditioned and difficult to solve. Therefore, a common remedy is to reduce the number of unknown elasticity values to $m \ll n$, thus generating a system where the number of parameters being optimized is reasonable given the number of available measurements.

Various techniques for reducing the number of unknown elasticity values exist. In short, it is most commonly accomplished via static imaging (inherent imaging characteristics, post-processing, and segmentation) or elastography. We rely on imaging to segment and group elements of similar morphology and thus mechanical properties, a strategy that has been harnessed by other researchers (Samani et al. 2003). Indeed, several imaging modalities are capable of distinguishing arterial and plaque components. In OCT, for instance, arterial geometries are reconstructed from images and then segmented (Fig. 1) (Chau et al. 2004). Yabushita et al. (2002) demonstrated that certain OCT imaging criteria, such as light backscattering, can, in fact, distinguish plaque morphology of diseased coronary arterial segments. When compared with correlating histological sections, plaque components were accurately partitioned and characterized due to increased soft tissue contrast as compared with IVUS. It should be noted that parameter reduction by image segmentation can be a source of error and that the accuracy of elasticity estimation inherently depends on the faithfulness of material boundary locations. In fact, this is an active area of research in medical imaging, and a detailed discussion of specific image segmentation processes and their potential errors is beyond the scope of present work.

Static images from some modalities are unable to differentiate tissue and plaque components consistently, and thus require further experimental studies. There is ongoing and extensive work, for instance, in utilizing elastography and resulting elastogram maps to characterize vascular tissue and plaque constituents, especially for IVUS (de Korte et al. 2003). Here, cross-correlation functions are applied to subsequent images of a tissue being externally displaced in order to track displacement or strain histories. And since changes in vascular tissue stiffness are indicative of varying elastic properties and pathological regions of interest, plaque detection has been proven possible. Recently, Lagrangian speckle model estimation has been applied

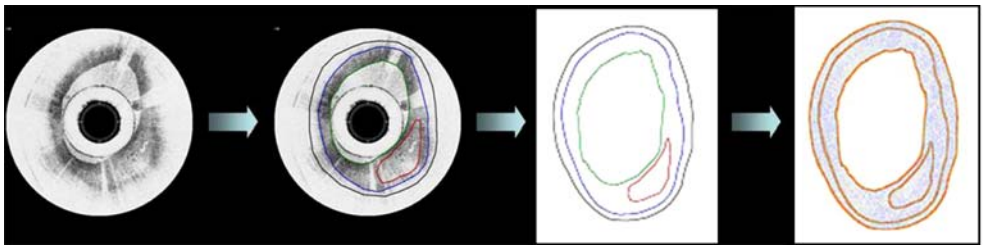

Fig. 1 OCT image of an arterial cross-section, segmented into plaque components, and meshed as a finite element model

to in vitro ultrasound elastography of excised human carotid artery and the resulting strain tensor showed promising plaque detection capability (Maurice et al. 2005). In fact, despite the increased soft tissue contrast afforded by OCT, we have complemented this modality with a multi-resolution variational framework for computing displacement and strain maps in vivo (Chau et al. 2004; Khalil et al. 2005). In summary, parameter reduction by image segmentation or elastography is feasible and has been previously proposed for generating lumped vascular finite element models, in particular, by tracing borders along high strain edges (Baldewsing et al. 2004).

Genetic algorithm

Genetic algorithms (GAs) are search methods that simulate biological evolution through naturally occurring genetic operations on chromosomes (Goldberg 1989; Holland 1975). They apply the Darwinian principle of survival of the fittest on string structures to build unique searches with elements of structure *and* randomness. Whereas the sole focus of traditional optimization is the *destination* of the search, the GA also values the *process of improvement* of a search.

Genetic algorithms begin with a predefined initial population of candidate solutions, typically created at random from a field of possible search solutions. Through pseudo- genetic operations, such as mating pool selection, crossover reproduction, and mutation, the ''fittest'' candidate solutions in the population survive to populate subsequent generation pools and facilitate the proliferation of new candidate solutions. Based on a simple set of rules and parameters dictating these genetic operations, the algorithm explores and learns the solution space efficiently.

The GA has been successfully applied to a wide array of optimization problems within economics, operations research, engineering, machine learning, ecology, population genetics, and social systems. It is an effective search algorithm in the context of complex, non-continuous solution spaces, especially those featuring multiple minima. It was even harnessed to determine the lowest energy structure of atomic clusters of carbon, remarkably finding fullerene as the optimal geometric structure of 60 carbons (Deaven and Ho 1995).

Algorithm design

The underlying skeleton of all genetic algorithms remains essentially identical, while the parameters governing the genetic operations are highly problem-specific. The first task is choosing how to represent the data and the population (P) of candidate solutions. In this case, we seek the optimal elastic modulus values for the lumped material regions given some mechanical responses. Therefore, a candidate solution is represented by an array of modulus values, one per lumped region. Typically, the GA is initialized by generating a distribution of solutions (elastic modulus values) at random and then assigning them to the candidates in the population, of chosen population size.

Next, we compute a fitness value for each candidate solution in the population; this quantifies how ''fit'' a candidate is as compared with others, in other words whether it is likely to survive and reproduce. The fitness measure is evaluated via an objective, or fitness, function. As stated above, inverse elasticity problems demand the minimization of a residual between measured and predicted displacement fields, thus we based our fitness function on Eq. (4):

$$f_i = \Phi(E_i), \tag{5}$$

where i represents a particular lumped material region and E_i is the vector of elasticity values for elements in that specific region.

With Eq. (5), a candidate solution is assigned fitness values for each lumped material region. After normalizing these values with respect to the number of elements per region, a *total fitness value* can be computed as the weighted sum,

$$F = \sum_i \alpha_i f_i, \tag{6}$$

of f_i, the normalized fitness values for lumped regions i, where α_i are normalized weighting factors that sum to 1. Initially and, in general, the fitness values were given equal weight; however, we discovered that empirically shifting the weights, in certain cases, could benefit the search.

For the purposes of this study, we next chose to implement relatively straightforward genetic operations that could later be expanded or adapted. A mating pool, or the group of candidate solutions picked to survive and reproduce, is selected by, first, ranking solutions according to fitness values. Subsequently, a survival probability is computed based on the rank:

$$\frac{((P+1)-\text{rank})^{\gamma}}{(1^{\gamma}+2^{\gamma}+\cdots+P^{\gamma})}, \tag{7}$$

where P is the population number and γ is an empirical factor that adjusts the curve to more or less favor ''fitter'' candidate solutions. Using Eq. (7), 50% of a generation is advanced into the mating pool ($P_{\text{mp}} = 0.5P$ where P_{mp} is the mating pool population), where $P_{\text{offspring}} = P_{\text{mp}}$ offspring are engendered via a crossover reproduction function that swaps elasticity values of two different candidate solutions at random. The offspring then join their parents to form the next generation of candidate solutions. The algorithm continues in this cyclic fashion, gradually learning the solution space until it has located the ''fittest'' solution(s) (Fig. 2).

A mutation operator was not implemented in this version of the algorithm, though future versions will incorporate it for added robustness. Random mutation will be a desired effect in the context of noisy data and computationally intensive problems. Here, we built randomness into larger initial population sizes and into the crossover reproduction operation.

Modeling

The FEM program ADINA (Watertown, MA) was used to solve for model displacements based on prescribed initial displacements, boundary conditions, model geometry, and material properties. Additionally, an integrated software package, tailored to interface with ADINA and optimize the elasticity parameters based on the above-described GA was developed.

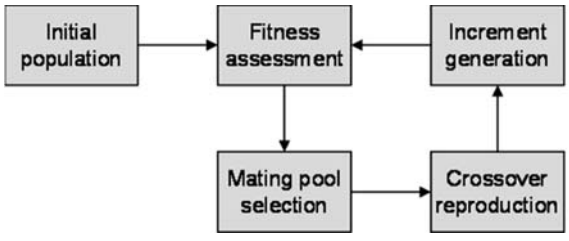

Fig. 2 Flowchart of genetic algorithm operations

The combined FEM/GA scheme was applied to several model problems, representing idealized arteries incorporating arterial plaques. Specifically, two-dimensional arterial cross-section models, with inner radius $r_i = 2$ mm and outer radius $r_o = 5$ mm, were built. A pressure of $p = 13.3$ kPa (100 mmHg), a mean physiologic arterial pressure, was applied to the inner lumens, consistent with realistic intravascular elastography experiments, where systemic blood pressure is exploited to deform the vessel. All the models satisfied the equilibrium equations for incompressible (Poisson's ratio $v = 0.499$), linear elastic solids undergoing small, quasi-static deformations and were meshed with 9-node quadrilateral elements. The measured displacement fields were generated by solving the forward problem with a given target elasticity field. White Gaussian noise was added to the displacement fields in certain cases. The set of candidate solutions was initially populated by randomly generating elasticity values within an order of magnitude of the target values, yielding initial populations of no less than 50 candidate solutions.

Results

Single inclusion models

To establish the validity of the algorithm, we first applied it to a model with 1 material region, or the one-parameter case (Fig. 3, left panel), and confirmed that it was able to locate the single elasticity value in one iteration. The two-parameter case, where a small circular inclusion was inserted in the idealized vascular model, was tested next (Fig. 3, right panel). Target E_2 modulus was varied between two values, representing two characteristic plaque constituents. In Simulation 1 the inclusion represents a hard calcified nodule surrounded by arterial fibrous plaque, while the inclusion in Simulation 2 models a soft lipid pool. For each simulation, the algorithm was initiated with candidate solution populations of 50.

From a relatively expansive range of initial candidate solutions (one order of magnitude), the algorithm converged on accurate approximations of the target values in 5 iterations (Table 1). In terms of computational time, the majority of the computation involved

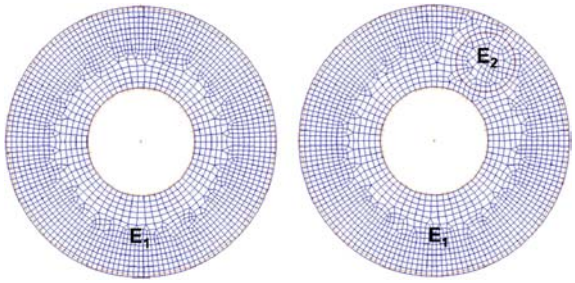

Fig. 3 One material region model consisting of 1844 elements (left panel) and two-parameter model consisting of 1710 elements in E_1 region and 103 elements in E_2 region (right panel)

solving the 250 total FEM forward problems, unlike in gradient-based methods where substantial computation is also required to generate a Jacobian matrix. A plot of the search history demonstrates the algorithm's rapid convergence on two elasticity values from an initial field of 50 (Fig.4). This behavior, where a diverse and large initial population is trimmed to a few candidate solutions, is characteristic of a successful GA scheme and illustrates the process of accelerated natural selection. Given a larger initial population and then allowing the algorithm respectively more time to craft accurate potential solutions with this larger initial set progressively eliminates the minor accuracy errors observed in the solutions of Table 1.

We next investigated the algorithm's ability to handle noise in the measured data. Specifically, different levels of white Gaussian noise, namely 0.3%, 1%, 5%, and 8%, were added to the displacement fields for the two-parameter, calcified arterial plaque model. The results confirmed that, despite noise levels of up to 8%, accurate and consistent lumped elasticity estimation from an initial population of 100 candidate solutions was possible (Fig. 5). Not surprisingly, the errors associated with the E_1 fibrous plaque region were consistently lower than those associated with the inclusion because, given the larger size of this region and the way the model was built, more displacement data was available here.

It must be remarked that the idealized problems presented above could be certainly treated within a gradient-based framework. The present alternative technique is however proposed because more complex solution spaces are not typically amenable to derivative approximations and usual tissue models are riddled with multiple inclusions of far-reaching elasticity values. In previous work done with gradient-based elasticity estimation, we successfully solved the discrete elasticity distribution for a tissue block model with one inclusion (Khalil et al. 2005). After reducing the number of elements to approximately 200, 10–20 iterations were required to converge on the discretized target elasticity field, yielding a total of 2000—4000 FEM forward problem solutions in addition to the computational time required to compute a Jacobian per iteration. While the model problems are not identical (i.e., in one case, we group together elements into material regions and, in the other, we solve for a distribution), it is still interesting to compare the outcomes of both techniques for, effectively, the single inclusion tissue model.

Multiple inclusion models

The transition to solving tissue models with multiple inclusions was relatively straightforward with the FEM/GA algorithm. When maintaining the same genetic operation constraints (population number, survival probability factor γ, etc.) as in the simpler model cases, solutions to models incorporating 3 or 4 material regions (Fig. 6) initially yielded mixed results, typically with one deviant elasticity result. The 4-parameter model is of specific physiological interest because a typical diseased arterial cross-section exhibits four morphological components: a thin layer of arterial wall surrounding a fibrous plaque region, with calcified and lipid inclusions.

In order to improve elasticity estimates while maintaining efficiency, we expanded the search in two ways. First, by increasing the population size and relaxing the restriction on iterations, the algorithm was allowed a more comprehensive exploration of the solution space. Second, the survival probability factor γ was adjusted in order to slow convergence. Specifically, decreasing γ (Eq. 7) eased the bias of selecting merely the ''fittest'' individuals, thereby preventing mating pools from becoming flooded with only a few candidate solutions too early in the search. Table 2 summarizes

Table 1 Convergence results for 2 material region models, representing plaques with a calcified inclusion (Simulation 1) and a lipid pool (Simulation 2). With an initial population of 50 candidate solutions, five iterations were needed to converge on accurate elasticity estimates

Simulation	$E_{1,\ \text{target}}$ [Pa]	$E_{2,\text{target}}$ [Pa]	$E_{1,\ \text{converged}}$ (error) [Pa]	$E_{2,\text{converged}}$ (error) [Pa]
1	6.00e5	3.00e7	6.14e5 (2.38%)	3.02e7 (0.68%)
2	6.00e5	3.00e3	5.96e5 (0.68%)	3.39e3 (12.9%)

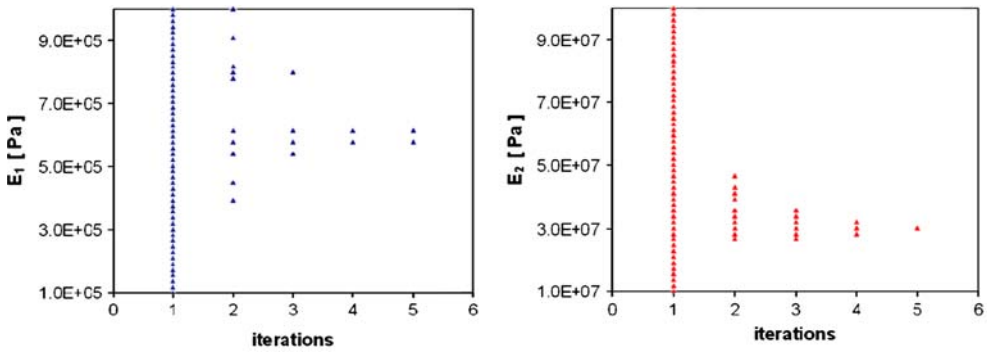

Fig. 4 Plot of Simulation 1 search history for each elastic modulus value. With an initial population of 50 candidate solutions, 5 iterations were needed to narrow the search to 1 or 2 potential solutions and then converge on E_1 (left panel) and E_2 (right panel)

the solution results upon adopting these search improvements: initial populations were enlarged to 100 individuals and, for the $m = 4$ parameter model, γ was gradually increased from an initial value of 0.5 to its default value of 1 over 5 iterations. The converged elasticity values and errors, as a result, returned to their target values and the convergence behavior, once again, became consistent. Furthermore, mapping stress distributions corresponding to a converged result (Fig. 7, left panel) alongside that of the target elasticity distribution (Fig. 7, right panel) confirms that, for such problems, it is possible to obtain the desired stress field. As expected, stress concentrations arise at the interface of large, compliant lipid pools and thin fibrous regions. It should be noted that slightly larger errors observed for softer (lower modulus) material regions are strictly an artifact of how we initiated the search algorithm. Recall that initial populations were generated from a range of within an order of magnitude of the target values. Therefore, if the initial candidate solutions for each material region are constrained to the same population number, then the interval steps for the softer material regions correspond to larger percent errors from the target value. Several potential remedies exist, and their implementation is problem-specific. We assumed a priori knowledge within an order of magnitude of the target elasticity values; however, in many cases, this range can be more precisely focused, thus diminishing errors associated with the initial population step size. Additionally, by including a random mutation operator that begets new candidate solutions, one can alleviate this initial population resolution error.

An alternative strategy we explored for improving solutions to the more complicated models was to empirically shift the weighting values α_i from their equally-weighted distribution. It was observed that fitness values (f_i) associated with stiffer regions (e.g., calcified nodules) were somewhat independent of the elasticity value of compliant regions (e.g., lipid pools). Therefore, giving fitness values of stiffer regions slightly more weight in their contribution to the total fitness value in earlier iterations, and then relaxing this restriction, yielded accurate elasticity estimates, as shown in Table 3 for a 3 material region model. As Fig. 8 demonstrates, the corresponding plot of search history reflected this weighting shift. We initiated α_3 to 0.9 and then decreased it to 0.3 after the first iteration. As a result, the algorithm converged on elasticity value E_3 more quickly than the others.

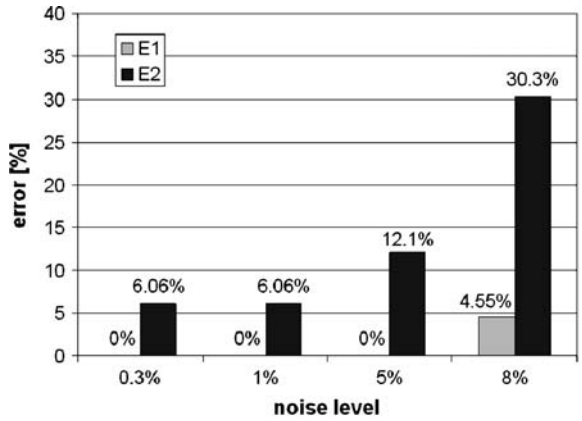

Fig. 5 Errors in $E_{converged}$ associated with adding 0.3%, 1%, 5%, and 8% white Gaussian noise to 'measured' displacement fields

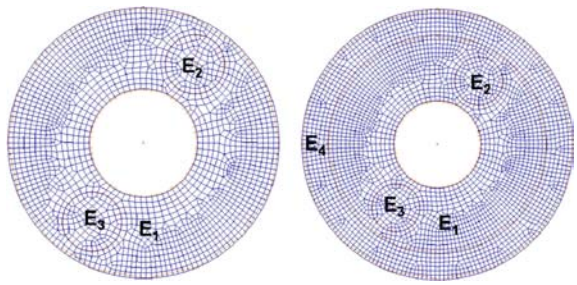

Fig. 6 Three material region model consisting of 1580, 103, and 102 elements in E_1, E_2, and E_3 regions (left panel) and four-parameter model consisting of 1580, 103, 102, and 1072 elements (right panel)

Table 2 Convergence results for 3 and 4 material region models where the searches were expanded in several ways. In the three-parameter model (m = 3), the initial population was increased to 100 candidate solutions. In the four-parameter model (m=4), the initial population was also increased to 100, and, in addition to this, the value of γ was systematically increased from 0.5 to 1

	E_{target} [Pa]	$E_{converged}$ (error) [Pa] (m = 3 model)	$E_{converged}$ (error) [Pa] (m = 4 model)
E_1	6.00e5	6.00e5 (0 %)	5.91e5 (1.52 %)
E_2	3.00e3	3.00e3 (0%)	3.18e3 (6.06%)
E_3	3.00e7	2.91e7 (3.03%)	3.00e7 (0%)
E_4	1.00e5	–	1.16e6 (16.4%)

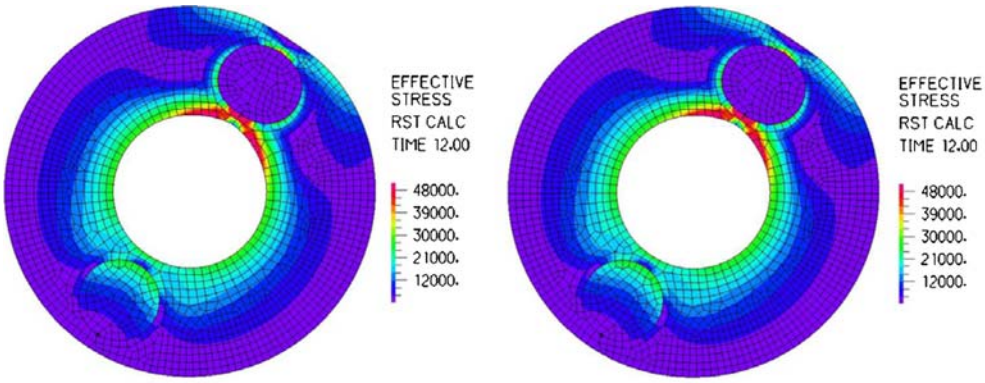

Fig. 7 Stress distributions corresponding to algorithm-converged elasticity values (left panel) and target elasticity values (right panel). Stress concentrations typically appear at the interface of large, compliant plaque components (i.e., lipid pools) and thin fibrous caps

Discussion

Soft tissue elasticity imaging and estimation is a challenging problem with clinical implications. For instance, it can aid with the identification of vulnerable intravascular plaques, which upon rupture very commonly lead to thrombosis and acute myocardial infarction. In fact, it is well known that rupture tends to occur in plaques possessing regions of high stress concentration (Richardson et al. 1989), thus the ability to reconstruct elasticity maps would be a valuable tool to complement plaque morphology maps.

Given internal tissue displacements that can be quantified from subsequent images of a specimen being deformed, tissue elasticity can be reconstructed using parameter estimation techniques. Typically, the inverse elasticity problem is posed and solved via an iterative, gradient-based search algorithm.

In some cases, gradient-based methods may be inadequate. The linear perturbation Gauss–Newton method, for instance, approximates the search gradient via serial perturbations of the modulus distribution. In complex and significantly inhomogeneous solution spaces a gradient is ineffective, especially when there are multiple minima. Additionally, these nonlinear least squares problems tend to be ill-conditioned, leading to inefficient or sometimes failing Newton direction searches. The Hessian matrix, the derivative of the gradient, is the matrix being inverted when solving the linear perturbation Gauss–Newton method for elasticity. Singular value decomposition (SVD) of this Hessian, however, reveals that due to a tendency for yielding large ratios of maximum to minimum singular values, ill-conditioning is an unavoidable concern. Furthermore, when formulating the Gauss–Newton method, the Hessian is simplified by omission of a second order term, which can further ill-condition the matrix to be inverted.

Table 3 Convergence results for a 3 material region model where the weighting factors α_i were used to bias the calcified inclusion (E_3) in earlier iterations

	E_{target} [Pa]	$E_{converged}$ (error) [Pa]
E_1	6.00e5	6.00e5 (0%)
E_2	3.00e3	3.27e3 (9.09%)
E_3	3.00e7	3.00e7 (0%)

An alternative technique was proposed here for the elasticity reconstruction problem. Upon image segmentation into plaque morphology, a combined FEM/GA algorithm can be implemented to yield the lumped elasticity values. The results presented, though from idealized models and data, confirm that such an approach has potential to accurately quantify elasticity, without explicitly approximating a gradient search direction, which requires considerable computational time. The algorithm was applied to models with increasing number of material regions, where the 4-parameter model was intended to reflect the notable morphological components of arterial plaques: arterial

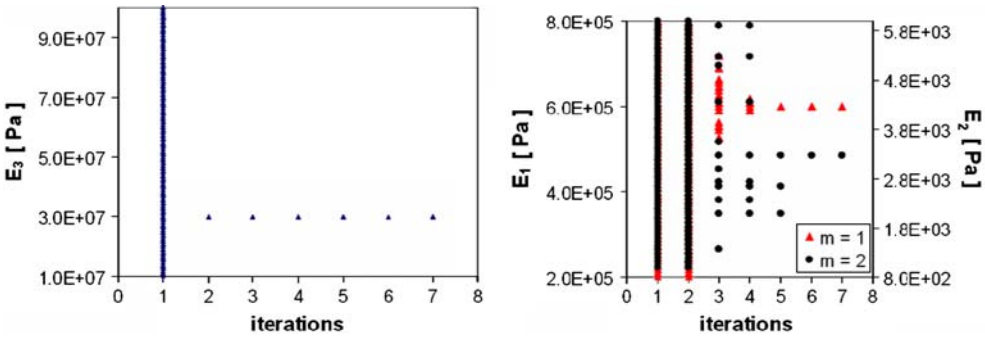

Fig. 8 Plot of search history for each elasticity value when weighting factors α_i were varied throughout the simulation. Slightly biasing the total fitness value toward the calcified inclusion, by increasing α_3 in earlier iterations, resulted in convergence of E_3, first, followed by convergence of E_1 and E_2

wall, fibrous plaque, lipid, and calcification. The results suggested that the present algorithm is capable of estimating multiple elasticity values for far-reaching modulus values, which can be difficult for gradient-based schemes in the context of smoothing.

It must be remarked that while pulsatile blood flow induces cyclic strain, which is believed to play a vital role in atherogenesis (Kaazempur-Mofrad et al. 2003), the focus of the present work was in elasticity estimation, we therefore assumed quasi-static deformations.

The present FEM/GA algorithm lends itself easily to future expansions and adaptations. It is a versatile approach to estimation for a broad range of material models, not merely isotropic, linear elastic. As a result, we have begun extending this technique to applications of anisotropic and nonlinear material models as well as 3D geometries, truly challenging problems for traditional elasticity estimation approaches. For one, the authors recognize that arterial tissue is generally very anisotropic and that the estimation results presented in this paper do not fully appreciate this observation (Vorp et al. 1995). Furthermore, simulations incorporating more physiological elasticity values and geometries would provide more biomechanical relevance in the future. The focus of this paper was on the development of a theoretical technique we feel has not yet been explored in the rapidly-growing field of tissue elasticity estimation. Due to its ease of implementation and robustness, a FEM/GA algorithm may serve as an effective low-resolution initial guess for discrete inverse formulations.

Acknowledgements The authors acknowledge fruitful discussions with Drs. Roger Kamm, Jung-Hoon Lee and Alireza Ghodrati. This study was funded by the National Institutes of Health (grant 5-R01-HL70039).

References

American Heart Association. Heart Disease and Stroke Statistics – 2003 Update. *American Heart Association* Dallas, TX, 2003.

Baldewsing RA, de Korte CL, Schaar JA, Mastik F, van der Steen AFW. A finite element model for performing intravascular ultrasound elastography of human atherosclerotic coronary arteries. Ultrasound Med Biol 2004;30:803–13

Cheng GC, Loree HM, Kamm RD, Fishbein MC, Lee RT. Distribution of circumferential stress in ruptured and stable atherosclerotic lesions. A structural analysis with histopathological correlation. Circulation 1993;87:1179–87

Chan RC, Chau AH, Karl WC, Nadkarni S, Khalil AS, Iftimia N, Shishkov M, Tearney GJ, Kaazempur Mofrad MR, Bouma BE. OCT-based arterial elastography: Robust estimation exploiting tissue biomechanics. Opt Express 2004;12:4558–72

Chau AH, Chan RC, Shishkov M, MacNeill B, Iftima N, Tearney GJ, Kamm RD, Bouma BE, Kaazempur-Mofrad MR. Mechanical analysis of atherosclerotic plaques based on optical coherence tomography. Ann Biomed Eng 2004;32:1494–503

Costa KD, Holmes JW, McCulloch AD. Modeling cardiac mechanical properties in three dimensions. Philos Trans R Soc Lond A 2001;359:1233–50

de Bray JM, Baud JM, Dauzat M, on behalf of the Consensus Committee. Consensus concerning the morphology and the risk of carotid plaques. Cereb Dis 1997;7:289–96

de Korte CL, van der Steen AFW, Céspedes EI, Pasterkamp G, Carlier SG, Mastik F, Schoneveld AH, Serruys PW, Bom N. Characterization of plaque components and vulnerability with intravascular ultrasound elastography. Phys Med Biol 2000;45:1465–75

de Korte CL, Schaar JA, Mastik F, Thijssen JM, van der Steen AFW. Cardiovascular Elastography. In:*Proc. World Congr. Ultrason*. Paris, France; 2003

Deaven DM, Ho KM. Molecular geometry optimization with a genetic algorithm. Phys Rev Lett 1995;75(2):288–91

Doyley MM, Meaney PM, Bamber JC. Evaluation of an iterative reconstruction method for quantitative elastography. Phys Med Biol 2000;45:1521–40

Duck FA. Physical properties of tissues—a comprehensive reference book. Sheffield, UK: Academic Press; 1990

Goldberg DE. Genetic algorithms in search, optimization, and machine learning. Boston, MA: Addison-Wesley Publishing Co., 1989

Holland JH. Adaptation in Natural and Artificial Systems. Ann Arbor: University of Michigan Press, MI, 1975

Humphrey JD. Mechanics of the arterial wall: review and directions. Crit Rev Biomed Eng 1995;23:82–90

Kaazempur-Mofrad MR, Younis HF, Patel S, Isasi AG, Chung C, Chan RC, Hinton DP, Lee RT, Kamm RD. Cyclic strain in human carotid bifurcation and its potential correlation to atherogenesis: idealized and anatomically-realistic models. J Eng Math 2003;47:299–314

Kallel F, Bertrand M. Tissue elasticity reconstruction using linear perturbation method. IEEE Trans Med Imaging 1996;15:299–313

Khalil AS, Chan RC, Chau AH, Bouma BE, Kaazempur Mofrad MR. Tissue elasticity estimation with optical coherence elastography: toward complete mechanical characterization of *in vivo* soft tissue. Ann Biomed Eng 2005;33(11):1631–1639

Loree HM, Tobias BJ, Gibson LJ, Kamm RD, Small DM, Lee RT. Mechanical properties of model atherosclerotic lesion lipid pools. Arterioscler Thromb 1994;14(2):230–4

Maurice RL, Brusseau E, Finet G, Cloutier G. On the potential of the Lagrangian speckle model estimator to characterize atherosclerotic plaques in endovascular elastography: *in vitro* experiments using an excised human carotid artery. Ultrasound Med Biol 2005;31(1):85–91

Mow VC, Kuei SC, Lai WM, Armstrong CG. Biphasic creep and stress relaxation of articular cartilage in compression: Theory and experiments. J Biomech Eng 1980;102:73–84

Oomens CWJ, Campen DH, Grootenboer HJ. A mixture approach to the mechanics of skin. J Biomech 1987;20:877–85

Ophir J, Céspedes EI, Ponnekanti H, Yazdi Y, Li X. Elastography: A quantitative method for imaging the elasticity in biological tissues. Ultrason Imaging 1991;13:111–34

Ophir J, Céspedes EI, Garra B, Ponnekanti H, Huang Y, Maklad N. Elastography: Ultrasonic imaging of tissue strain and elastic modulus *in vivo*. Eur J Ultrasound 1996;3:49–70

Ponnekanti H, Ophir J, Huang Y, Céspedes I. Fundamental mechanical limitations on the visualization of elasticity contrast in elastography. Ultrasound Med Biol 1995;21:533–43

Richardson PD, Davies MJ, Born GVR. Influence of plaque configuration and stress distribution on fissuring of coronary atherosclerotic plaques. Lancet 1989;8669:941–4

Samani A, Bishop J, Luginbuhl C, Plewes DB. Measuring the elastic modulus of *ex vivo* small tissue samples. Phys Med Biol 2003;48:2183–98

Sarvazyan A. Shear acoustic properties of soft biological tissues in medical diagnostics. In Proc Acoust Soc Am Ottawa, Canada 1993

Skovoroda AR, Emelianov SY, O'Donnell M. Reconstruction of tissue elasticity based on ultrasonic displacement and strain images. IEEE Trans Ultrason Ferroelectr Freq Control 1995;42:747–65

Vorp DA, Rajagopal KR, Smolinski PJ, Borovetz HS. Identification of elastic properties for orthotropic vascular segments in distension. J Biomech 1995;28:501–12

Yabushita H, Bouma BE, Houser SL, Aretz T, Jang I, Schlendorf KH, Kauffman CR, Shishkov M, Kang D, Halpern EF, Tearney GJ. Characterization of human atherosclerosis by optical coherence tomography. Circulation 2002;106:1640–45

Yuan C, Tsuruda JS, Beach KN, Hayes CE, Ferguson MS, Alpers CE, Foo TK, Strandness DE. Techniques for high-resolution MR imaging of atherosclerotic plaque. J Mag Res Imag 1994;4:43–9